TGF-β-induced activation of mTOR complex 2 drives epithelial–mesenchymal transition and cell invasion

Samy Lamouille[1], Erin Connolly[2], James W. Smyth[3], Rosemary J. Akhurst[2,4] and Rik Derynck[1,2,4,5,*]

[1]Department of Cell and Tissue Biology, [2]Helen Diller Family Comprehensive Cancer Center, [3]Cardiovascular Research Institute, [4]Department of Anatomy, [5]Program in Developmental Biology, University of California at San Francisco, San Francisco, CA 94143-0512, USA

*Author for correspondence (rik.derynck@ucsf.edu)

Accepted 16 October 2011
Journal of Cell Science 125, 1259–1273

doi: 10.1242/jcs.095299

Summary

In cancer progression, carcinoma cells gain invasive behavior through a loss of epithelial characteristics and acquisition of mesenchymal properties, a process that can lead to epithelial–mesenchymal transition (EMT). TGF-β is a potent inducer of EMT, and increased TGF-β signaling in cancer cells is thought to drive cancer-associated EMT. Here, we examine the physiological requirement for mTOR complex 2 (mTORC2) in cells undergoing EMT. TGF-β rapidly induces mTORC2 kinase activity in cells undergoing EMT, and controls epithelial cell progression through EMT. By regulating EMT-associated cytoskeletal changes and gene expression, mTORC2 is required for cell migration and invasion. Furthermore, inactivation of mTORC2 prevents cancer cell dissemination in vivo. Our results suggest that the mTORC2 pathway is an essential downstream branch of TGF-β signaling, and represents a responsive target to inhibit EMT and prevent cancer cell invasion and metastasis.

Introduction

In cancer progression, carcinoma cells escape the site of the primary tumor through their ability to degrade extracellular matrix, migrate and colonize remote sites via lymphatic and blood vessel routes (Nguyen and Massagué, 2007). It is thought that epithelial–mesenchymal transition (EMT), a reversible cellular reprogramming process that is accompanied with cell shape and behavior changes, initiates carcinoma dissemination (Thiery and Sleeman, 2006).

During EMT, cells disassemble their epithelial junctions and repress the expression of junctional proteins, some of which mark epithelial identity. Prominently, E-cadherin, a component of adherens junctions, is lost during EMT and cancer progression (Thiery and Sleeman, 2006; Zeisberg and Neilson, 2009). Cells undergoing EMT also increase expression of mesenchymal proteins and matrix metalloproteases (MMPs), which promote cell invasion (Zeisberg and Neilson, 2009). Complementing the switch in gene expression, cells undergoing EMT alter their morphology and reorganize their actin cytoskeleton. The switch of actin from cortical architecture to stress fibers associated with focal adhesion complexes enhances the ability of the cell to migrate (Yilmaz and Christofori, 2009).

Transforming growth factor-β (TGF-β) has emerged as a potent inducer of EMT, and induces EMT of cells in culture, allowing for dissection of signaling that leads to EMT (Miettinen et al., 1994; Zavadil and Böttinger, 2005; Moustakas and Heldin, 2007; Miyazono, 2009; Xu et al., 2009). Increased production of active TGF-β by tumor cells, and increased TGF-β receptor levels, resulting in autocrine TGF-β signaling, are thought to induce or be required for EMT of carcinoma cells in vivo (Bierie and Moses, 2006a; Padua and Massagué, 2009).

TGF-β signals through tetrameric complexes of transmembrane dual-specificity kinase receptors, and Smad proteins which translocate into the nucleus to regulate transcription (Shi and Massagué, 2003; Feng and Derynck, 2005). Upon TGF-β activation, Smads control the expression and activities of transcription factors involved in EMT such as Snail (Snai1), which represses transcription of the E-cadherin gene (Zavadil and Böttinger, 2005; Moustakas and Heldin, 2007; Xu et al., 2009). TGF-β receptors also activate non-Smad signaling, such as MAPK pathways, PI3K, and Rho GTPase signaling (Derynck and Zhang, 2003; Moustakas and Heldin, 2005). Activation of RhoA is involved in dissolving epithelial junctions, reorganizing the actin cytoskeleton and effecting cell shape changes during EMT (Bhowmick et al., 2001; Ozdamar et al., 2005).

In cells that undergo EMT in response to TGF-β, TGF-β induces rapid activation of PI3K, Akt, mTOR complex 1 (mTORC1) and S6 kinase, leading to increases in protein synthesis, cell size, motility and invasion (Lamouille and Derynck, 2007). In addition to mTORC1, which is composed of mTOR, Raptor, mLST8, and PRAS40, mTOR complex 2 (mTORC2), has been identified (Jacinto et al., 2004; Sarbassov et al., 2004) and comprises mTOR, mLST8, Rictor, mSIN1 and Protor (Laplante and Sabatini, 2009). The roles of mTORC2 remain poorly defined. mTORC2 phosphorylates Akt on Ser473 (Sarbassov et al., 2005), which, together with Akt phosphorylation on Thr308 by PDK1 in response to PI3K activation, confers full activity to Akt. The identification of Rictor and mSIN1 as essential for mTORC2 function allows studies on the roles of mTORC2 through targeted attenuation of their expression (Frias et al., 2006; Guertin et al., 2006; Jacinto et al., 2006; Shiota et al., 2006; Yang et al., 2006).

We now address the role of mTORC2 in TGF-β-induced EMT. We show that TGF-β rapidly induces mTORC2 kinase activity. Although not required for the epithelial phenotype, mTORC2 is required for cells to complete EMT in response to TGF-β. Without Rictor, the cells are arrested in an intermediate stage

Journal of Cell Science

between epithelial and mesenchymal differentiation, without the motile and invasive behavior of cells after EMT. Loss of mTORC2 activity blocks cancer cell dissemination and the formation of metastatic nodules in a mouse model. Our results show that mTORC2 is a novel and crucial mediator in TGF-β signaling, which might serve as a target for the prevention of and cancer metastasis.

Results

TGF-β induces mTORC2 kinase activity and enhances mTORC2 formation during EMT

Mouse mammary epithelial NMuMG cells are commonly used as model to study TGF-β-induced EMT. As these cells are very responsive to TGF-β, they also represent a valuable model to study TGF-β-activated signaling pathways. We first determined whether TGF-β induces mTORC2 activity in these cells. As shown in Fig. 1A, TGF-β induced phosphorylation of Akt at Ser473, which was detectable 15 minutes after the addition of TGF-β, and was maintained for up to 75 minutes, in parallel with phosphorylation of Akt at Thr308. The increase in Akt(S473) phosphorylation correlated with an increase in mTORC2 kinase activity, starting after 15 minutes, as shown by an in vitro kinase assay (Fig. 1B). This activation was dependent on TβRI receptor kinase and PI3K activities because SB431542, an inhibitor of the TβRI kinase, and LY294002, an inhibitor of PI3K, blocked TGF-β-induced mTORC2 activation (Fig. 1B). GDC-0941, a specific inhibitor of the class IA PI3K, similarly blocked the TGF-β-induced Akt(S473) phosphorylation, confirming the role of PI3K in the induction of mTORC2 kinase activity by TGF-β (Fig. 1C).

TGF-β-induced EMT is completed in 36 hours in NMuMG cells (Miettinen et al., 1994). Because the major morphological changes in EMT occur after 12 hours of TGF-β treatment, we extended our analyses to 24 hours. Formation of the mTORC2 complex, detected by Rictor co-immunoprecipitation with mTOR and mLST8, was not enhanced by 15 or 45 minutes of TGF-β treatment (Fig. 1D, top), but increased after 18 hours and 21 hours. This increase was blocked by SB431542, but not by LY294002. The enhanced mTORC2 formation at 18 and 21 hours was accompanied by increased phosphorylation of Akt(S473) and Akt(T308), which was lower than the rapid increase in Akt phosphorylation at 15 minutes or 45 minutes, and was blocked by both SB431542 and LY294002 (Fig. 1D, bottom). These data indicate that TGF-β treatment enhances mTORC2 formation and Akt phosphorylation later during TGF-β-induced EMT, at the time of the cytoskeletal and cell morphology changes.

TGF-β-induced Akt(S473) phosphorylation is dependent on mTORC2 activity

To determine whether mTORC2 mediates TGF-β-induced phosphorylation of Akt(S473), we stably downregulated the expression of Rictor or mSIN1, which are both components of mTORC2, using lentiviral shRNA expression. The substantial decrease in Rictor expression obtained using two distinct shRNAs (sh#1 or sh#2), or in mSIN1 expression, abrogated TGF-β-induced Akt(S473) phosphorylation and inhibited the phosphorylation of the Akt substrate GSK-3β (Fig. 2A). Downregulation of Rictor or mSIN1 expression also decreased phosphorylation of Akt(T308) in NMuMG cells, as observed in other cell models (Sarbassov et al., 2005; Yang et al., 2006), but did not affect TGF-β-induced mTORC1 activation, as detected by phosphorylation of ribosomal protein S6 (Fig. 2A) or Smad3 (Fig. 2B). Downregulation of Rictor expression with Rictor sh#1 also decreased mSIN1 expression to similar levels as achieved with mSIN1 shRNA. Conversely, silencing of mSIN1 expression only slightly decreased Rictor expression (Fig. 2A). As reported previously (Frias et al., 2006; Jacinto et al., 2006), these results indicate that downregulation of Rictor expression affects the stability of mSIN1 in mTORC2.

The integrin-linked kinase (ILK) was reported to phosphorylate Akt(S473) in some cell types, and Rictor was found to interact with ILK, enhancing ILK-induced Akt (S473) phosphorylation (McDonald et al., 2008). However, downregulation of ILK expression using siRNA did not affect TGF-β-induced Akt(S473) phosphorylation in NMuMG cells (Fig. 2C). Moreover, TGF-β induced Ser473 phosphorylation of both Akt1 and Akt2, and downregulation of Rictor expression inhibited both phosphorylation events (Fig. 2D). Similarly to the rapid activation of mTORC2 in response to TGF-β, downregulation of Rictor expression also inhibited TGF-β-induced Akt(S473) as well as Akt(T308) phosphorylation, at 18 hours and 21 hours (Fig. 2E), and decreased the TGF-β-induced GSK-3β phosphorylation at 18 hours and 21 hours (Fig. 2F). Together, these results demonstrate that mTORC2 is activated in response to TGF-β and mediates TGF-β-induced Akt(S473) phosphorylation, independently of Smad3, and that TGF-β enhances Akt activation dependent on mTORC2 at a later stage of TGF-β-induced EMT.

mTORC2 activity is required for TGF-β-induced EMT

We evaluated the role of mTORC2 in TGF-β-induced EMT by characterizing the effects of downregulating Rictor expression using Rictor sh#1, the most efficient shRNA to downregulate Rictor, in NMuMG cells. Repression of Rictor expression did not affect the epithelial morphology in the absence of TGF-β (Fig. 3A, supplementary material Fig. S1A). In addition, no change in cortical actin organization or E-cadherin localization at cell junctions was observed compared with that in control cells (Fig. 3B).

Treatment of NMuMG cells with TGF-β resulted in EMT, with a change from cobblestone to elongated cell shape, reorganization of cortical actin into stress fibers, and membrane delocalization and downregulation of E-cadherin expression (Fig. 3A,B). By contrast, decreased Rictor expression dramatically impaired the TGF-β-induced EMT of NMuMG cells (Fig. 3A,B, supplementary material Fig. S1A). The cells maintained an epithelial morphology, with some colocalization of E-cadherin and cortical actin, indicative of epithelial cell–cell contacts, in contrast to the EMT phenotype of control cells. Similar results were obtained using stable lentiviral expression of Rictor sh#2 or shRNA that targets mSIN1 (supplementary material Fig. S1B,C). After 48 hours of treatment with TGF-β, Rictor-knockdown cells did not acquire a spindle morphology and were still somewhat epithelial, but with reduced colocalization of actin and E-cadherin at cell–cell junctions (Fig. 3A,B, supplementary material Fig. S1A,B). We previously reported that mTORC1 is activated in TGF-β-induced EMT (Lamouille and Derynck, 2007). Rapamycin treatment, which inhibits mTORC1 activity, did not interfere with the inhibition of

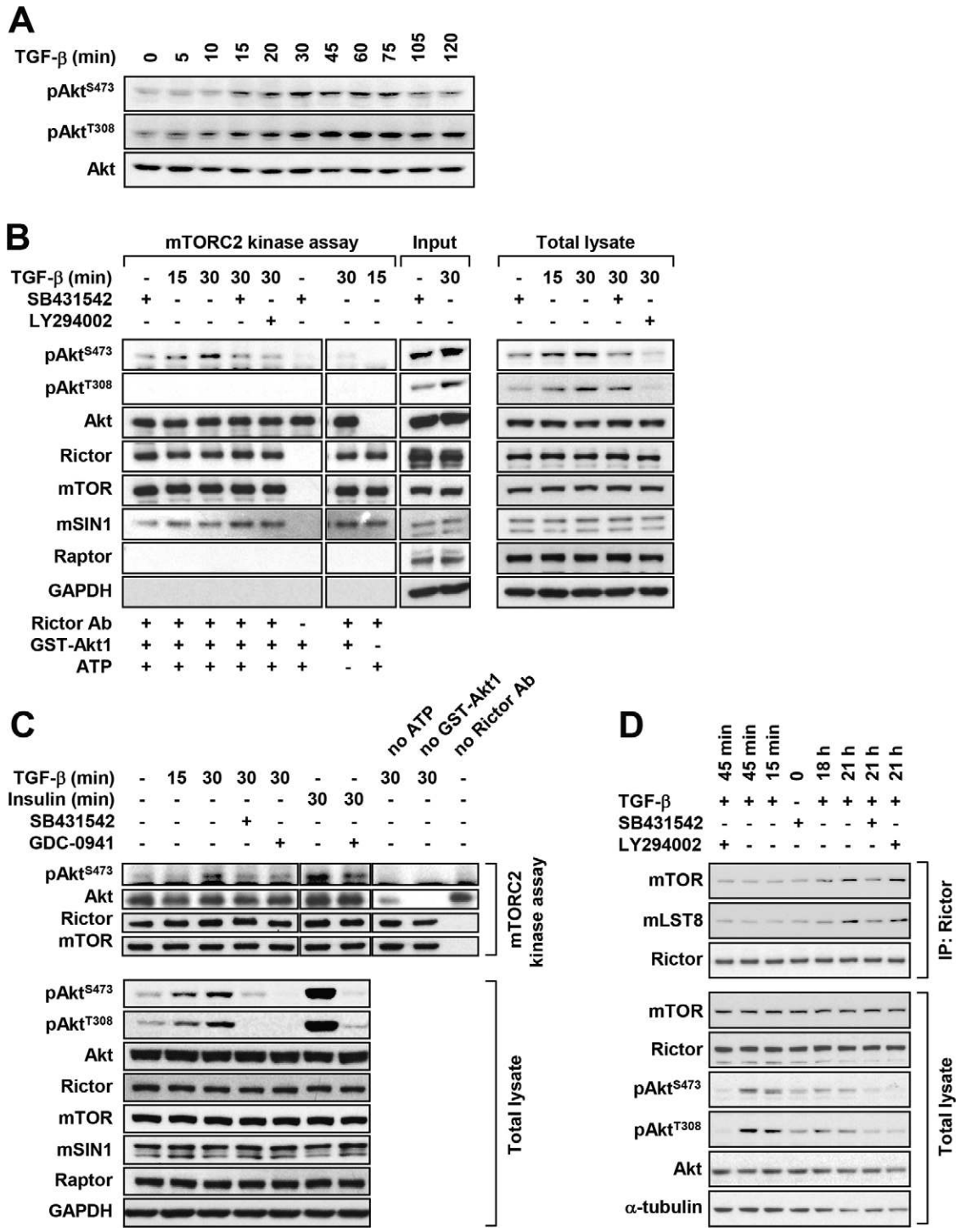

Fig. 1. TGF-β induces mTORC2 activation. (**A**) NMuMG cells were treated with TGF-β for the indicated times before lysis and immunoblotting. (**B**) NMuMG cells were treated or not with TGF-β for the indicated times, in the presence or absence of SB431542 or LY294002. Cell lysates were subjected to anti-Rictor immunoprecipitation, and the immunoprecipitates were subjected to in vitro kinase assays using kinase-inactive Akt1 as a substrate, before immunoblotting of the kinase reactions, immunoprecipitates and cell lysates. The left panels are from the same gel, without differential exposure. (**C**) NMuMG cells were treated or not with TGF-β or insulin for the indicated times, in the presence or absence of SB431542 or GDC-0941. The kinase activity of mTORC2 was then assessed as in B. The top panels are from the same gel, without differential exposure. (**D**) NMuMG cells were treated or not with TGF-β for the indicated times, in the presence or absence of SB431542 or LY294002. Cell lysates were subjected to immunoprecipitation using Rictor antibody, and/or immunoblotted.

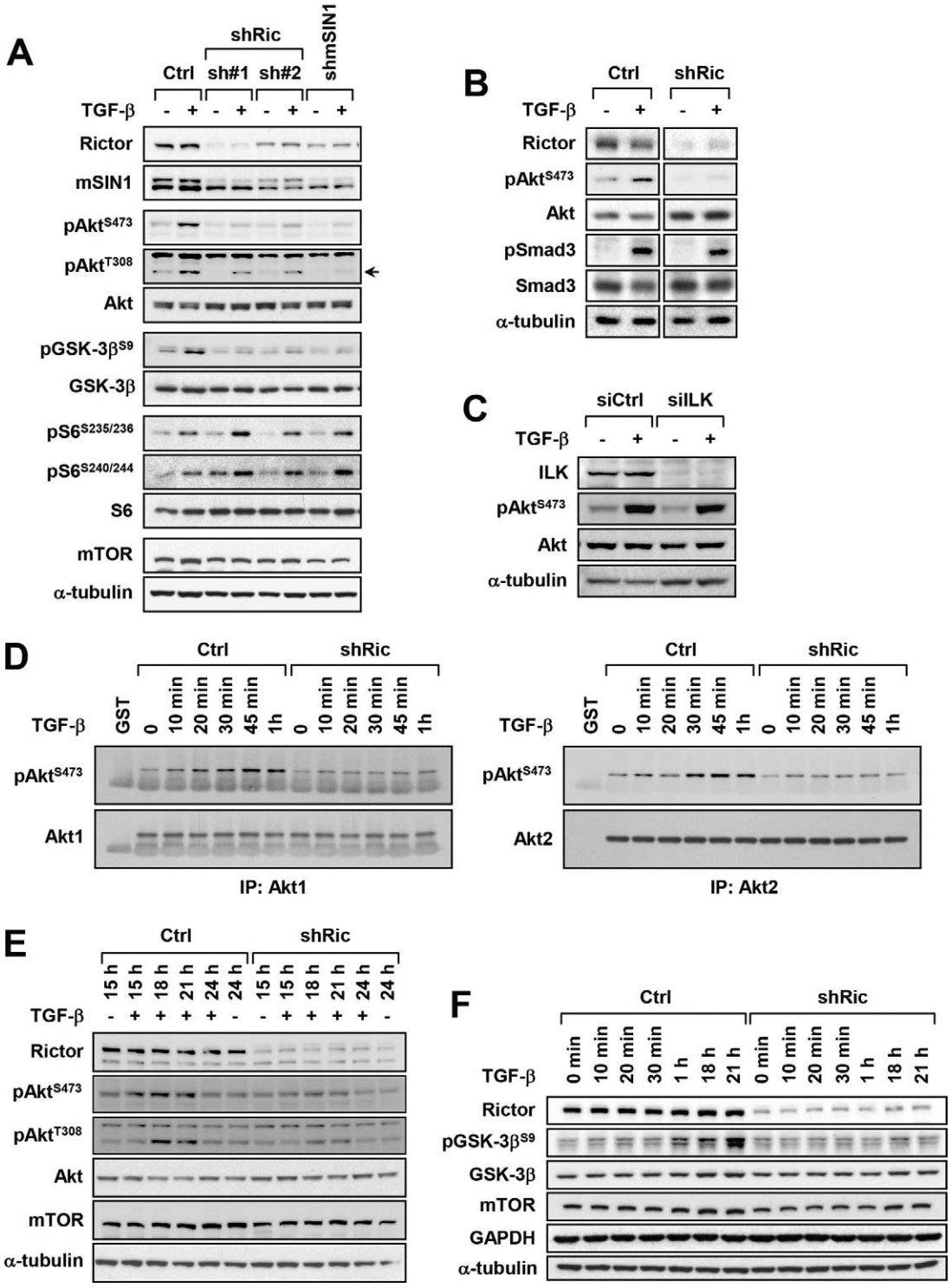

Fig. 2. Downregulation of Rictor expression suppresses TGF-β-induced mTORC2 activation. (**A**) NMuMG cells expressing shRNA against Rictor (shRic, sh#1 or sh#2), mSIN1 (shmSIN1) or control (Ctrl), were treated or not with TGF-β for 1 hour before lysis and immunoblotting. (**B**) Control or Rictor-knockdown NMuMG cells were treated with TGF-β for 1 hour before lysis and immunoblotting. The panels are from the same gel, without differential exposure. (**C**) NMuMG control (siCtrl) cells or cells expressing siRNA to downregulate ILK (siILK) were treated or not with TGF-β for 1 hour before lysis and immunoblotting. (**D**) Control or Rictor-knockdown NMuMG cells were treated with TGF-β for the indicated times before lysis, immunoprecipitation with Akt1 or Akt2 antibodies, and immunoblotting. (**E**,**F**) Control or Rictor-knockdown NMuMG cells were stimulated or not with TGF-β for the indicated times before lysis and immunoblotting.

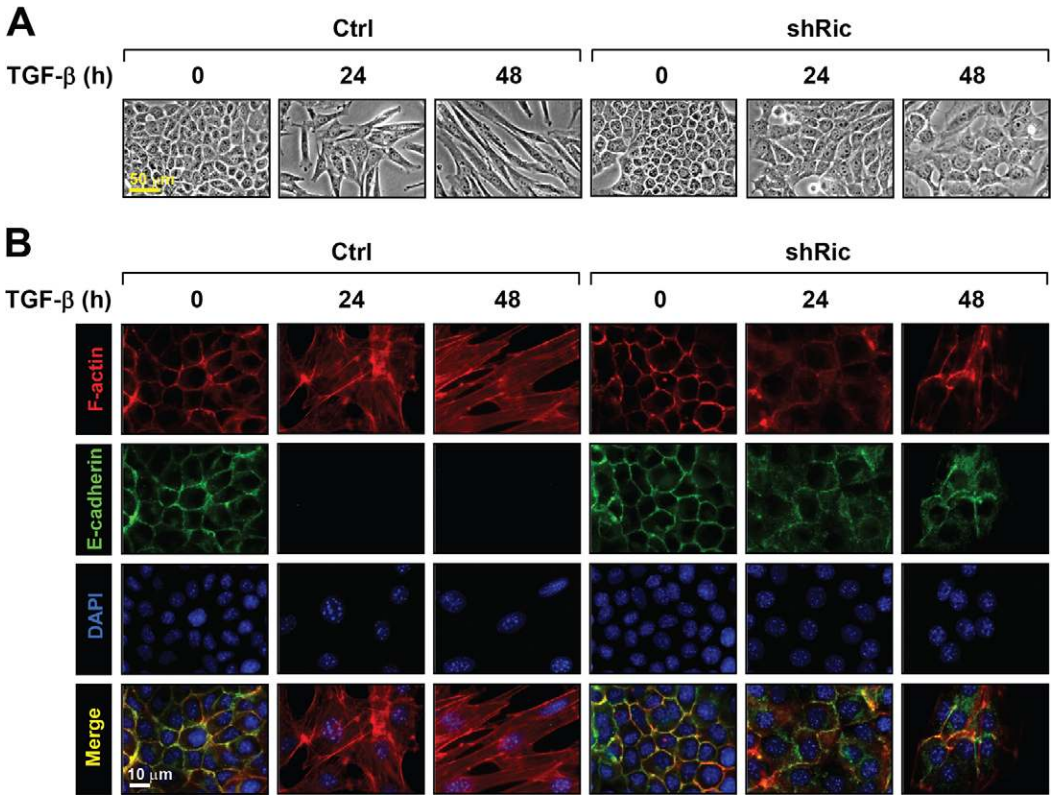

Fig. 3. Inhibition of mTORC2 activity blocks TGF-β-induced EMT of NMuMG cells. (**A**,**B**) Control or Rictor-knockdown NMuMG cells were treated with TGF-β for the indicated times and observed by phase-contrast microscopy (A), or subjected to staining for F-actin, immunostaining for E-cadherin, and DAPI staining to visualize nuclei (B). Scale bars: 50 μm (A) and 10 μm (B).

TGF-β-induced EMT by Rictor downregulation (supplementary material Fig. S1D).

mTORC2 activity regulates marker gene expression in TGF-β-induced EMT

To further characterize the role of mTORC2, we analyzed the downregulation of E-cadherin expression during EMT in NMuMG cells. Compared with control cells, the TGF-β-induced downregulation of E-cadherin protein (Fig. 4A, supplementary material Fig. S1E) and RNA (Fig. 4B) expression were incomplete in Rictor-knockdown cells. Similar results were obtained using Rictor sh#2 or mSIN1 shRNA (supplementary material Fig. S1F,G). Moreover, the TGF-β-induced increase in N-cadherin expression was much lower in Rictor-knockdown cells, compared with control cells (Fig. 4A). EMT is accompanied by the induction of expression of Snail, a transcription factor that binds E-cadherin promoter sequences, repressing E-cadherin transcription. The rapid induction of expression of *Snai1* mRNA by TGF-β was reduced by 40% in cells with downregulated Rictor expression (Fig. 4C). This effect on Snail expression was confirmed using Rictor sh#2 or mSIN1 shRNA (supplementary material Fig. S1H,I). To evaluate the contribution of Akt1 and Akt2, downstream of mTORC2 activity, in TGF-β-induced *Snai1* transcription, we transfected NMuMG cells with siRNAs that specifically downregulated the expression of Akt1 or Akt2 (Fig. 4D). Both siAkt1 and siAkt2 inhibited TGF-β-induced transcription of *Snai1* (Fig. 4E). To evaluate whether this effect on Snail expression contributed to the inhibition of TGF-β-induced EMT in Rictor-knockdown cells, we stably downregulated Snail expression. Snail expression was robustly decreased at the protein and mRNA level (Fig. 4F,G). As a result, decreased Snail expression inhibited TGF-β-induced EMT in NMuMG cells, which was apparent by the maintenance of an epithelial morphology (Fig. 4H).

We conclude that, in NMuMG cells, mTORC2 is required for TGF-β-induced EMT, and that inhibition of mTORC2 activity, or decreased Akt1 or Akt2 expression, attenuates the changes in gene expression that mediate EMT.

mTORC2 is required for cytoskeletal reorganization, RhoA activation and cell migration in TGF-β-induced EMT

Reorganization of actin from a cortical pattern to stress fibers is a hallmark of EMT (Yilmaz and Christofori, 2009), and NMuMG cells undergo such cytoskeletal reorganization in response to TGF-β (Miettinen et al., 1994). To better visualize the actin in individual cells, we expressed GFP-tagged actin in control and Rictor-knockdown NMuMG cells. The cells were seeded sparsely, and live-cell imaging was undertaken on isolated cells. Control cells had completed EMT 48 hours after addition of TGF-β, resulting in isolated and elongated cells with longitudinal actin stress fibers connected to the cell cortex (Fig. 5A). By contrast, Rictor-knockdown cells retained an epithelial shape, and GFP-tagged actin remained predominantly cortical (Fig. 5A). In addition, these cells had significantly lower stress fiber density as determined by linear profile analysis (Fig. 5B, left), and fewer

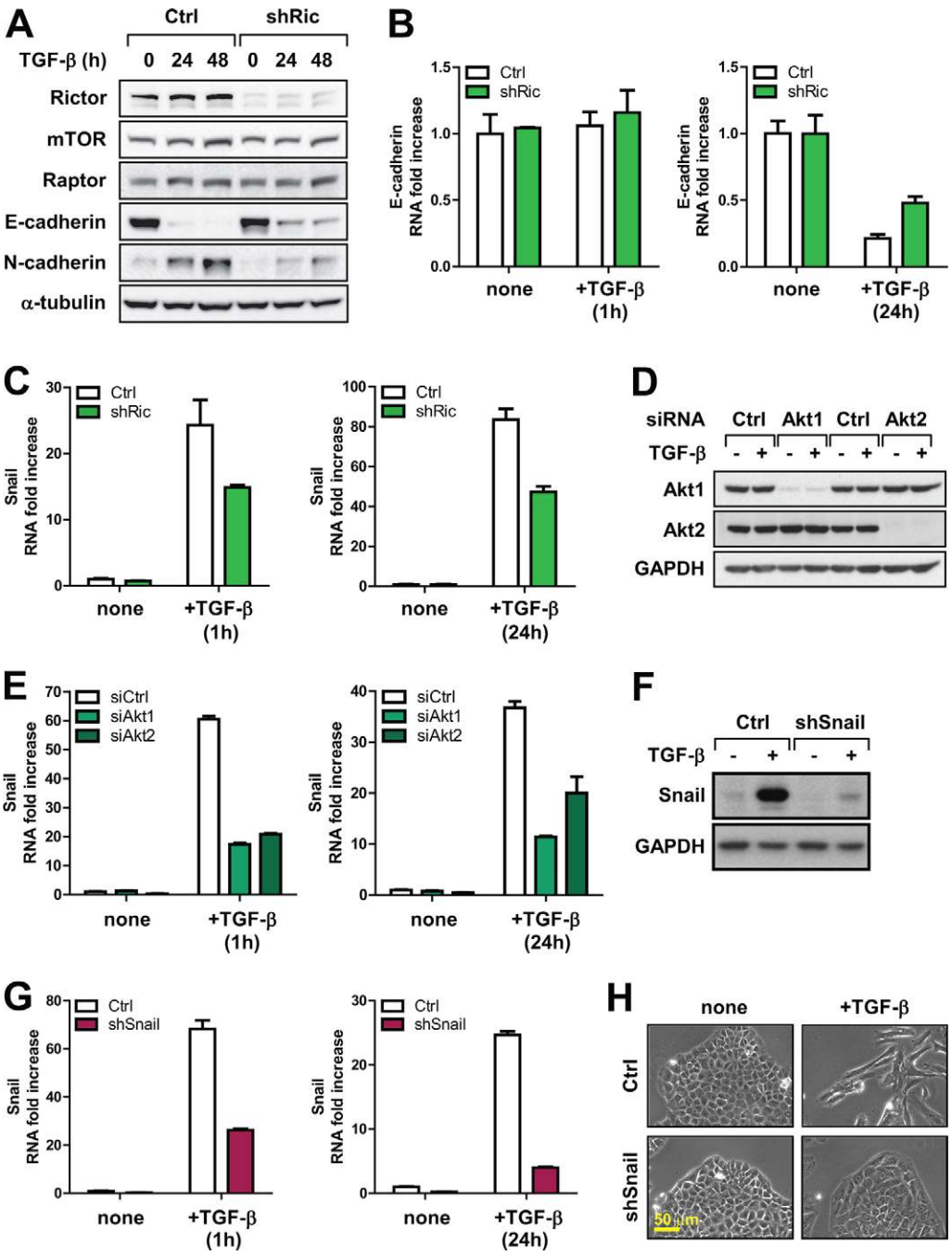

Fig. 4. Inhibition of mTORC2 activity attenuates TGF-β-induced changes in EMT marker expression. (**A**) Control or Rictor-knockdown NMuMG cells, treated with TGF-β for the indicated times, were lysed and analyzed by immunoblotting. (**B**,**C**) Control or Rictor-knockdown NMuMG cells were treated or not with TGF-β for 1 hour or 24 hours, RNA was extracted and levels of mRNA encoding E-cadherin (B) or Snail (C) were quantified by qRT-PCR. Error bars show mean ± s.e.m. (**D**) NMuMG cells expressing siRNA against Akt1 (siAkt1), Akt2 (siAkt2) or control (siCtrl), were treated or not with TGF-β for 1 hour before lysis and immunoblotting. (**E**) NMuMG cells expressing siAkt1, siAkt2, or siCtrl were treated or not with TGF-β for 1 hour or 24 hours. RNA was extracted and *Snai1* mRNA levels were quantified by qRT-PCR. Error bars show mean ± s.e.m. (**F**) NMuMG cells expressing shRNA against Snail (shSnail) or GFP (Ctrl), were treated or not with TGF-β for 48 hours before lysis and immunoblotting. (**G**) Control and Snail-knockdown NMuMG cells were treated or not with TGF-β for 1 hour or 24 hours, RNA was extracted and *Snai1* mRNA levels were quantified by qRT-PCR. Error bars show mean ± s.e.m. (**H**) Control and Snail-knockdown NMuMG cells were treated or not with TGF-β for 48 hours, and observed by phase-contrast microscopy. Scale bar: 50 μm.

stress fibers interacting with the cell cortex. Using circular statistical analysis to study stress fiber alignment, the mean resultant length (*R*), a measure of uniformality of orientation from 0 (random) to 1 (total alignment), was significantly lower in Rictor-knockdown cells than in control cells (Fig. 5B, right), confirming the perturbed stress fiber organization following TGF-β treatment.

Reorganization of actin into stress fibers during EMT is regulated by Rho-GTPases such as RhoA (Yilmaz and Christofori, 2009). Both TGF-β and mTORC2 have been implicated in regulating RhoA activity (Bhowmick et al., 2001; Jacinto et al., 2004). In control cells, TGF-β induced GTP loading of RhoA within 10 minutes. In Rictor-knockdown cells, however, RhoA–GTP remained at basal levels (Fig. 5C). These results demonstrate that TGF-β-induced RhoA activation requires mTORC2, and that mTORC2 regulates actin reorganization during TGF-β-induced EMT, most likely through regulation of RhoA activity.

Cells that have undergone EMT in response to TGF-β display enhanced migration. Because downregulation of Rictor expression inhibited TGF-β-induced actin reorganization in EMT, we compared the motility of control and Rictor-knockdown cells. Monolayers of control and Rictor-knockdown NMuMG cells, pretreated with TGF-β for 48 hours to induce EMT, were scratched, and wound closure was observed for 24 hours in the absence of TGF-β (Fig. 5D, left). Control cells

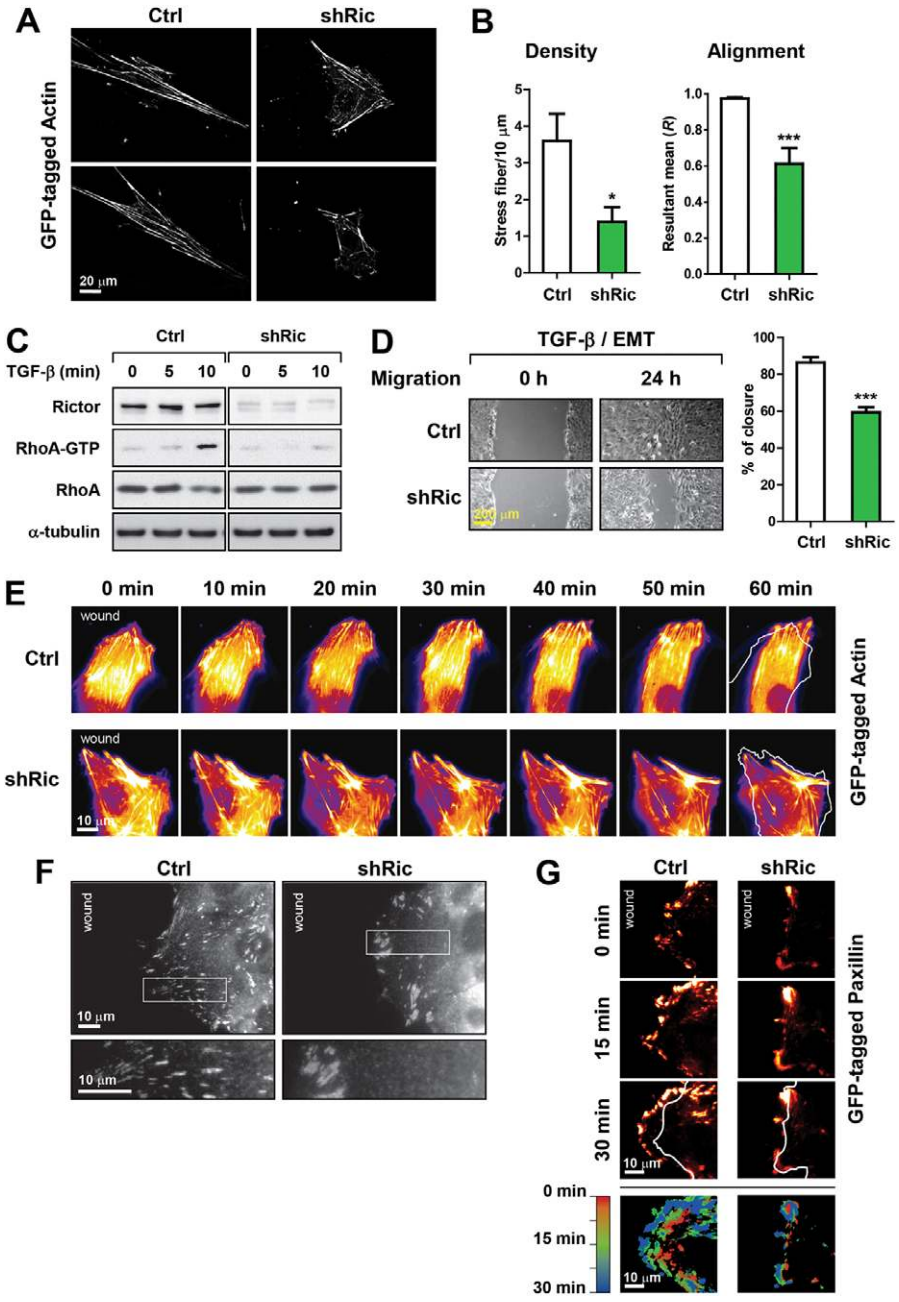

Fig. 5. Inhibition of mTORC2 activity inhibits the actin reorganization and migration of NMuMG cells. (**A**) Control or Rictor-knockdown NMuMG cells expressing GFP-tagged actin, were treated with TGF-β for 48 hours, trypsinized, and seeded sparsely before live-cell real-time epifluorescence imaging. Scale bar: 20 μm. (**B**) Actin stress-fiber density was quantified from linear fluorescence intensity profiles of lines drawn through the cell body (left panel), and stress fiber angles were determined with circular statistical analysis performed to generate mean resultant length (R) as a quantitative readout of stress fiber orientation in individual cells (Ctrl, $n=8$; shRic, $n=7$; 1=total alignment, 0=random in graph of alignment). Error bars represent mean ± s.e.m. $^{*}P<0.05$; $^{***}P<0.001$. (**C**) Control or Rictor-knockdown NMuMG cells were stimulated with TGF-β for the indicated times. Active GTP-bound RhoA was isolated using GST–Rhotekin-RBD–Sepharose, and detected by immunoblotting using antibody against RhoA. Total lysates were immunoblotted with antibodies against Rictor, RhoA or α-tubulin. The two panels are from the same gel, without differential exposure. (**D**) Control or Rictor-knockdown NMuMG cells were treated with TGF-β for 48 hours. Cell migration was observed at 0 and 24 hours after wounding, in the absence of TGF-β. Scale bar: 200 μm. The percentage of wound closure was calculated at 24 hours by the mean of eight wound widths per condition performed in triplicates. Error bars show mean ± s.e.m. $^{***}P<0.001$. (**E**) Control or Rictor-knockdown NMuMG cells expressing GFP-tagged actin were observed by live-cell real-time epifluorescence imaging of GFP-tagged actin (pseudocolor) 3 hours after wounding, in absence of TGF-β. Panels are 200 msecond acquisitions at 10 minute time intervals for a total of 60 minutes. White outlines show the cell cortex at $t=0$. Scale bar: 10 μm. (**F**) Control or Rictor-knockdown NMuMG cells were immunostained for paxillin 6 hours after wounding, in absence of TGF-β. The bottom two panels represent an enlargement of the white outlined rectangles. Scale bar: 10 μm. (**G**) Control or Rictor-knockdown NMuMG cells expressing GFP-tagged paxillin were observed by live-cell real-time TIRFm imaging of GFP-tagged paxillin (pseudocolor) 3 hours after wounding, in the absence of TGF-β. The top six panels are 200 msecond acquisitions at 15 minute time intervals. White outlines show the cell cortex at $t=0$. The bottom two panels are pseudocolored z projections of the entire time course. Scale bar: 10 μm.

that had undergone EMT after TGF-β pretreatment achieved 86% wound closure, and silencing of Rictor expression resulted in decreased cell migration (Fig. 5D, right). Expression of GFP-tagged actin permitted real-time visualization of changes in actin organization in migrating cells (supplementary material Movies 1, 2). In control cells, actin stress fibers were aligned with the direction of migration and interacted with the cell cortex at the wound edge (Fig. 5E, top). A highly dynamic polymerization of actin stress fibers allowed the cells to move into the wound. By contrast, the actin cytoskeleton was disorganized and less dynamic in Rictor-knockdown cells, and these cells did not migrate efficiently (Fig. 5E, bottom). We also examined the microtubule organization by α-tubulin immunofluorescence in the same assay. Microtubules were poorly organized and less linear in Rictor-knockdown cells compared with control cells. (supplementary material Fig. S2A). Efficient cell migration depends not only on the actin cytoskeleton, but also on dynamics of focal adhesions, allowing migrating cells to adhere at the leading edge and detach at the trailing edge. Immunofluorescence for paxillin in migrating cells visualized focal adhesion localization and shape (Deakin and Turner, 2008). In control cells, paxillin was evenly distributed at the leading edge in a punctate pattern that is characteristic of focal adhesions (Fig. 5F, left). By contrast, downregulation of Rictor expression conferred an irregular paxillin distribution, often in larger patches (Fig. 5F, right). Using cells expressing GFP-tagged paxillin, we observed focal adhesion dynamics by live-cell time-lapse imaging (supplementary material Movies 3, 4). Rictor-knockdown cells had markedly perturbed GFP-tagged paxillin dynamics at the leading edge, in comparison to control cells (Fig. 5G). These results illustrate that mTORC2 functions in the regulation of actin and focal adhesion dynamics required for migration of cells undergoing TGF-β-induced EMT.

mTORC2 is required for TGF-β-induced invasion and MMP9 expression

Cells that have undergone EMT acquire an invasive behavior. We analyzed whether mTORC2 is involved in the increased invasion of NMuMG cells following TGF-β-induced EMT using an invasion assay in Matrigel-coated Transwell chambers. Control cells that had undergone EMT in response to TGF-β were highly invasive compared with untreated cells. Decreased Rictor expression resulted in significantly reduced invasion after 48 hours of TGF-β (Fig. 6A), which was confirmed using Rictor sh#2 or mSIN1 shRNA (supplementary material Fig. S2B,C).

The invasive behavior following EMT depends upon increased activity of MMPs, such as MMP2 and MMP9, which degrade the surrounding matrix (Kessenbrock et al., 2010), and TGF-β is known to regulate expression of these MMPs (Zavadil and Böttinger, 2005). Accordingly, TGF-β strongly induced the activity of MMP9 in NMuMG cells, as assessed by zymography (Fig. 6B). Induction of MMP9 activity was blocked by the TβRI inhibitor SB431542. Decreased Rictor expression repressed the induction of MMP9 activity in response to TGF-β, with no change in TGF-β-induced Smad3 phosphorylation (Fig. 6B). The repression of MMP9 activity correlated with decreased *Mmp9* mRNA expression in response to TGF-β (Fig. 6C). The reduction in *Mmp9* mRNA was confirmed using mSIN1 shRNA (supplementary material Fig. S2D). To evaluate the contribution of Akt1 and Akt2 in TGF-β-induced MMP9 expression, we stably downregulated the expression of Akt1 or Akt2 in NMuMG, using lentiviral shRNA (Fig. 6D). Knockdown of Akt1 or Akt2 expression inhibited the TGF-β-induced increase in *Mmp9* mRNA (Fig. 6E). Moreover, knockdown of Snail expression using shRNA, also blocked the TGF-β-induced increase in *Mmp9* mRNA (Fig. 6F). NMuMG cells had low levels of MMP2 activity compared with MMP9, and MMP2 activity was decreased in the presence of TGF-β. Downregulation of Rictor expression did not affect MMP2 activity (Fig. 6B).

To evaluate the role of MMP9, NMuMG cells were transfected with siRNA against MMP9, which abrogated the TGF-β-induced increase in *Mmp9* mRNA (Fig. 6G) and MMP9 activity (Fig. 6H). Decreased MMP9 expression resulted in a substantial reduction in invasion of cells that had undergone EMT in response to TGF-β (Fig. 6I). We conclude that MMP9 is a key effector in the invasion of NMuMG cells that have undergone EMT in response to TGF-β, and that the induction of MMP9 expression requires mTORC2, as well as Akt1 or Akt2, and Snail, which function downstream from mTORC2. These results define mTORC2 as a regulator of cell invasion in TGF-β-induced EMT.

mTORC2 is required for spindle tumor formation and carcinoma dissemination of squamous carcinoma cells

To study the role of mTORC2 in TGF-β-dependent EMT during cancer progression, we used E4 squamous carcinoma cells, originally derived from a lymph node metastasis of a skin carcinoma (Burns et al., 1991). E4 cells are squamous in culture and undergo a reversible TGF-β-induced EMT to a full spindle cell phenotype. When implanted subcutaneously, E4 cells grow as a spindle cell carcinoma that depends on TβRII signaling for prevention of a squamous reversion (Portella et al., 1998). The use of E4 cells allowed us to study the role of mTORC2 in EMT in vitro and in vivo, and cancer dissemination in vivo. In response to TGF-β, E4 cells in culture changed from an epithelial morphology to scattered stellate cells with loss of cell–cell contacts after 48 hours (supplementary material Fig. S3A). After TGF-β treatment, cortical actin was reorganized into stress fibers, and E-cadherin dissipated from the cell junctions, which are both characteristics of EMT (supplementary material Fig. S3B). SB431542 blocked TGF-β-induced EMT in E4 cells.

We downregulated Rictor expression in E4 cells by stable lentiviral expression of Rictor shRNA. Decreased Rictor expression in TGF-β-treated cells inhibited the activity of mTORC2, shown by inhibition of Akt(S473) phosphorylation, and decreased Akt(T308) phosphorylation without a change in Smad3 phosphorylation (Fig. 7A). As in NMuMG cells, knockdown of Rictor expression did not affect the epithelial phenotype, but inhibited the completion of TGF-β-induced EMT after 48 hours, observed by the absence of cell scattering and maintenance of cell–cell contacts (Fig. 7B). Additionally, cortical actin did not reorganize into stress fibers in response to TGF-β, and E-cadherin remained localized at cell–cell junctions (Fig. 7C). The TGF-β-induced decrease in E-cadherin expression (Fig. 7D), and induction of Snail (Fig. 7E) and MMP9 (Fig. 7F) expression were attenuated in Rictor-knockdown E4 cells as observed in NMuMG cells. Moreover, the invasion of E4 cells upon TGF-β-induced EMT was impaired in cells expressing Rictor shRNA (Fig. 7G). These results illustrate that in E4 cells, mTORC2 is required for TGF-β-induced EMT into spindle invasive cells, and invasion.

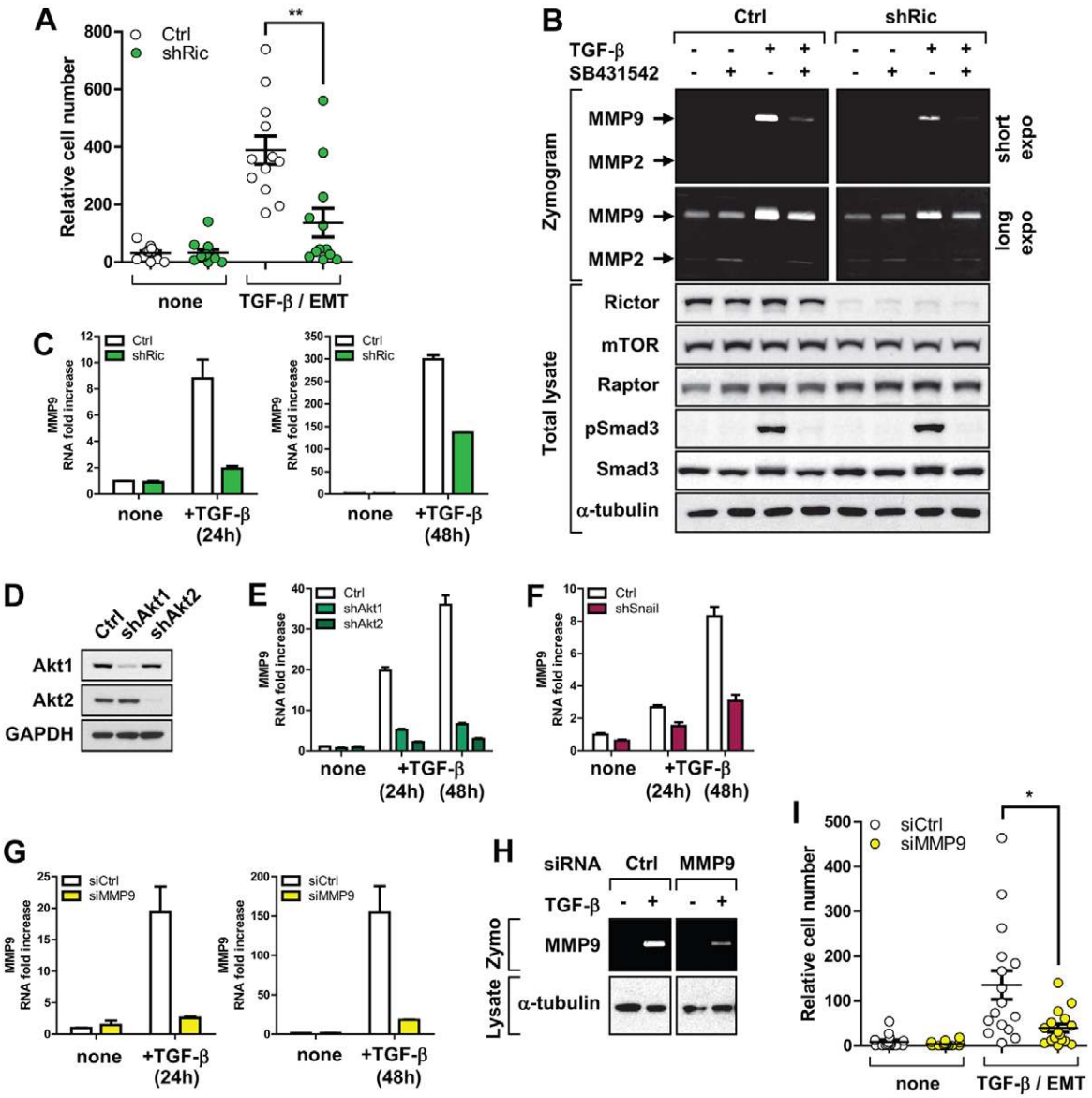

Fig. 6. Inhibition of mTORC2 activity decreases NMuMG cell invasion. (**A**) Control or Rictor-knockdown NMuMG cells treated or not with TGF-β for 48 hours, were placed in Matrigel-coated Transwell chambers. After 24 hours, the DAPI-stained nuclei on the lower surface were counted in four fields per filter in triplicate. Error bars show mean ± s.e.m. $^{**}P<0.01$. (**B**) Control or Rictor-knockdown NMuMG cells were treated with or without SB431542 for 1 hour, and TGF-β was added or not for 24 hours. The supernatants were analyzed by gelatin zymography, and cell lysates were immunoblotted. The two top panels are from the same gel, without differential exposure. (**C**) NMuMG cells expressing shRNA to Rictor, or control were treated or not with TGF-β for 24 or 48 hours. RNA was extracted and *Mmp9* mRNA levels were quantified by qRT-PCR. Error bars show mean ± s.e.m. (**D**) NMuMG cells expressing shRNA to Akt1 (shAkt1), Akt2 (shAkt2) or GFP (Ctrl), were subjected to lysis and immunoblotting. (**E**–**G**) NMuMG cells expressing shRNA to Akt1, Akt2 or control (E), shRNA to Snail or control (F), or siRNA against MMP9 (siMMP9), or siCtrl (G), were treated or not with TGF-β for 24 or 48 hours. RNA was extracted and *Mmp9* mRNA levels were quantified by qRT-PCR. Error bars show mean ± s.e.m. (H, I) NMuMG cells were transfected with siMMP9 or siCtrl. In (**H**), the cells were treated or not with TGF-β for 24 hours. The supernatants were analyzed by gelatin zymography (Zymo), and cell lysates (Lysate) were immunoblotted with antibody against α-tubulin. The two panels are from the same gel, without differential exposure. (**I**) Cells were treated or not with TGF-β for 48 hours, and invasion was assessed as in A. The DAPI-stained nuclei were counted in eight fields per filter in duplicate. Error bars show mean ± s.e.m. $^{*}P<0.05$.

Because mTORC2 activity is required for TGF-β induced EMT, we also examined the effect of attenuating Rictor expression in carcinoma cells that have completed EMT and are, accordingly, more invasive. For this purpose, we used the spindle carcinoma D3 cells, derived from the same carcinoma that gave rise to E4 cells. These fibroblastoid cells show constitutive Ras activation and TGF-β signaling. Similarly to many other cancer cell lines, D3 cells have a constitutive Akt(S473) phosphorylation, and addition of TGF-β only slightly increased this phosphorylation (supplementary material Fig. S4A). Stable knockdown of Rictor expression using shRNA abrogated Akt(S473) phosphorylation without inhibiting Akt(T308) phosphorylation, with or without TGF-β treatment (supplementary material Fig. S4A). D3 cells with reduced Rictor

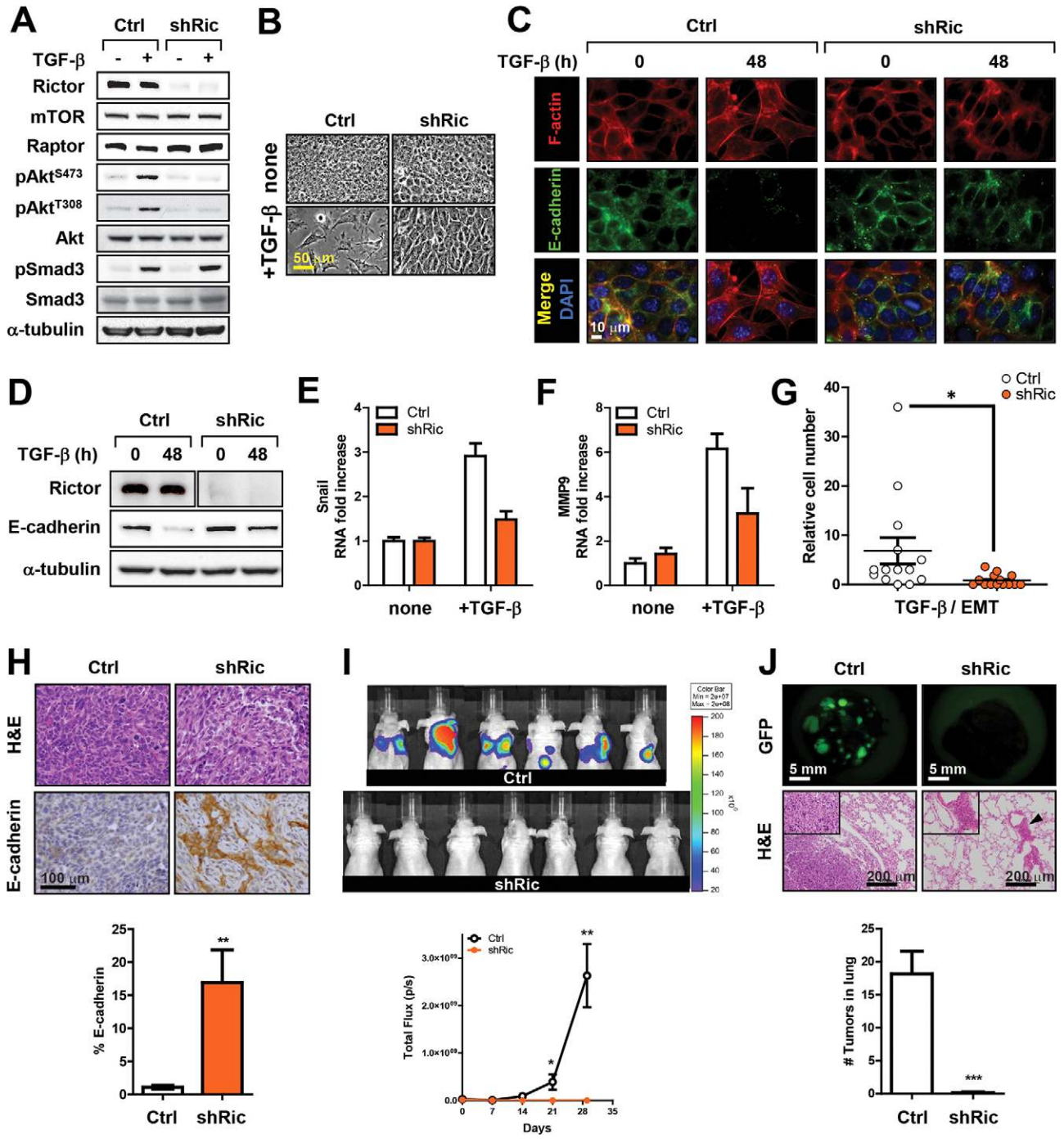

Fig. 7. Inhibition of mTORC2 blocks TGF-β-induced EMT and invasive behavior of E4 squamous carcinoma cells. (**A**) Control or Rictor-knockdown E4 cells were treated with TGF-β for 1 hour before lysis and immunoblotting. (**B**–**D**) Control or Rictor-knockdown E4 cells were treated or not with TGF-β for 48 hours and observed by phase-contrast microscopy (B), stained for F-actin and immunostained for E-cadherin, with nuclei visualized by DAPI staining (C), or lysed and immunoblotted (D) (the two top panels are from the same gel, without differential exposure). Scale bars: 50 μm (B) and 10 μm (C). (**E**,**F**) Control or Rictor-knockdown E4 cells were treated or not with TGF-β for 1 hour (E) or 48 hours (F). RNA was extracted and *Snai1* (E) or *Mmp9* (F) mRNA levels were quantified by qRT-PCR. Error bars show mean ± s.e.m. (**G**) Control or Rictor-knockdown E4 cells were treated with TGF-β for 48 hours, and placed in Matrigel-coated Transwell chambers. After 24 hours, the DAPI-stained nuclei on the lower surface were counted in seven fields per filter in duplicate. Error bars show mean ± s.e.m. $*P<0.05$. (**H**) Histological evaluation of subcutaneous xenografts of control or Rictor-knockdown E4 cells 21 days after injection into nude mice. Scale bar: 100 μm. The percentage of tumor cells positive for E-cadherin staining is shown in the histogram. Error bars represent mean ± s.e.m. $**P<0.01$. (**I**) IVIS Luminas-quantified bioluminescence, 29 days after tail vein injection of luciferase- and GFP-labeled control or Rictor-knockdown E4 cells into nude mice. The bottom graph shows a quantification of bioluminescence over time. Error bars represent mean ± s.e.m. $*P<0.05$; $**P<0.01$. (**J**) Ex-vivo fluorescence stereo microscope imaging of lungs from nude mice, 29 days after tail vein injection of luciferase- and GFP-labeled control or Rictor-knockdown E4 cells. Scale bar: 5 mm. Lower panels are representative H&E-stained images of sections through the lungs with enlargement pictures in the top left corners. Arrowhead indicates a micrometastasis around a blood vessel. Scale bar: 200 μm. The bottom graph shows quantification of GFP-positive foci in the lungs. Error bars represent mean ± s.e.m. $***P<0.001$.

expression were less elongated (supplementary material Fig. S4B), expressed less fibronectin than control cells (supplementary material Fig. S4C), and showed a substantial decrease in cell migration, measured by wound closure (supplementary material Fig. S4D). Both MMP2 and MMP9 were constitutively active in D3 cells, and decreased Rictor expression inhibited their activity (supplementary material Fig. S4E). Finally, D3 cells showed a highly invasive behavior, and, reflecting their high autocrine TGF-β activity, the invasiveness was only moderately enhanced in response to TGF-β (supplementary material Fig. S4F). By contrast, knockdown of Rictor expression inhibited the invasion of D3 cells, with or without TGF-β pretreatment. We conclude that mTORC2 has an important role in the maintenance of the spindle fibroblastoid phenotype of D3 cells, and, consistent with our results using NMuMG cells, plays a key role in cancer cell invasion through regulation of MMP2 and MMP9 expression.

E4 cells readily form spindle tumors when injected subcutaneously. To examine the role of mTORC2 in the TGF-β-dependent spindle carcinoma phenotype in vivo, we subcutaneously injected nude mice with control or Rictor-knockdown cells, and allowed tumor formation for 3 weeks. The tumors maintained the downregulated Rictor expression, as shown by immunoblotting or immunofluorescence (supplementary material Fig. S5A,B). They were also histologically examined by hematoxylin and eosin (H&E) staining or immunohistochemistry for E-cadherin (Fig. 7H). Consistent with their spindle carcinoma phenotype, tumors that developed from control cells were largely devoid of E-cadherin expression, presumably a result of local TGF-β signaling in the tumor micro-environment. By contrast, tumors with decreased Rictor expression had large areas of cells with squamous morphology and membrane-localized E-cadherin (Fig. 7H, supplementary material Fig. S5C). These data are consistent with the role of mTORC2 in TGF-β-induced downregulation of E-cadherin and EMT of E4 and NMuMG cells in culture, and confirm that, in vivo, mTORC2 is required for repression of E-cadherin expression. Downregulation of Rictor expression slightly decreased proliferation of E4 cells in tumors, and did not significantly affect cell death, as quantified by BrdU (supplementary material Fig. S5D) and TUNEL (supplementary material Fig. S5E) staining.

To assess the role of Rictor in the metastatic behavior of carcinoma cells, we generated E4 control and Rictor-knockdown cells stably expressing luciferase and EGFP. Cells were injected into the tail vein of nude mice, to follow the formation of metastatic nodules within the lungs. An equal number of control or Rictor-knockdown E4 cells was injected, and verified by bioluminescence imaging 1 hour after injection (data not shown). Mice were monitored every 2 days, and evaluated by bioluminescence once per week. Whereas all mice receiving control cells developed bioluminescent metastases in the lungs, no metastases were detected in mice injected with Rictor-knockdown cells (Fig. 7I). Lungs were harvested and analyzed using fluorescence stereo-microscopy to detect GFP-positive nodules 29 days after cell injection. Consistent with the bioluminescence results, lung nodules were detected in all control mice, but not in mice injected with Rictor-knockdown cells (Fig. 7J). H&E staining confirmed the presence of metastases in the lungs of control mice, but not in mice injected with Rictor-knockdown cells. A few micro-metastases were detected around blood vessels in the lungs of mice injected with Rictor-knockdown cells, but there was a dramatic reduction in dissemination of the shRictor cells (Fig. 7J, arrowhead). These effects were principally the consequence of inhibition of cell invasion rather than inhibition of proliferation or cell survival, because cell proliferation and death did not significantly differ between control and Rictor-knockdown cells in the lungs (supplementary material Fig. S5F,G). Taken together, we observed a dramatic decrease in metastatic behavior of Rictor-knockdown cells when compared with control cells, indicating that mTORC2 is required for the metastatic potential in this model.

Discussion

Signaling of autocrine TGF-β secreted by tumor cells is increasingly seen as driving cancer progression, related to its ability to induce EMT in carcinoma cells, which contributes to invasion and metastasis (Bierie and Moses, 2006b; Nguyen and Massagué, 2007). We found that mTORC2 is a target of TGF-β signaling, and addressed its role in the induction of EMT by TGF-β (Fig. 8). We show that mTORC2 activity is not required for the epithelial phenotype, but mediates the progression of EMT and invasion in cell culture and in vivo. Our findings present novel insights into the complexities of TGF-β signaling and the EMT process, and an avenue for targeted intervention in carcinoma progression.

mTORC2 activity is required for EMT, but not for the epithelial phenotype

Downregulating mTORC2 activity has no effect on the epithelial phenotype in cell culture. By contrast, mTORC2 is required for epithelial cells to acquire a mesenchymal phenotype in response to TGF-β. The lack of effect on epithelial cells is consistent with a recent report that mTORC2 is required for the development of prostate cancer caused by *Pten* deficiency in epithelial cells, but not in normal prostate epithelial cells (Guertin et al., 2009).

EMT results from a set of sequential changes that lead to disassembly of epithelial cell junctions, loss of epithelial phenotype, acquisition of mesenchymal characteristics and shape, and increased motility and invasion (Thiery and Sleeman, 2006). Careful observation led to the proposal that cells undergo EMT through an unstable state in which they express both epithelial and mesenchymal markers, before displaying an increased migratory and invasive behavior (Klymkowsky and Savagner, 2009). Our observations suggest that Rictor-knockdown cells treated with TGF-β are arrested in this intermediate state, and, thus, that mTORC2 is required for the transition into the mesenchymal, invasive phenotype. While mTORC2 is involved in the initiation of TGF-β-induced EMT, for example by regulating early transcription responses, it is also involved in a second signaling wave, where increased interaction between Rictor and mTOR and changes in cell morphology and behavior occur. Tumors contain a small population of self-regenerating cells that give rise to the bulk of the tumor. These cells might arise in part from EMT or share characteristics of cells that have undergone EMT (Thiery et al., 2009). Our finding that mTORC2 is required for EMT might contribute to understanding the properties of these cancer stem cells. Additionally, a recent report suggested a role for mTORC2 in the phenotype of SW480 colon cancer cells, with decreased Rictor expression resulting in increased expression of E-cadherin

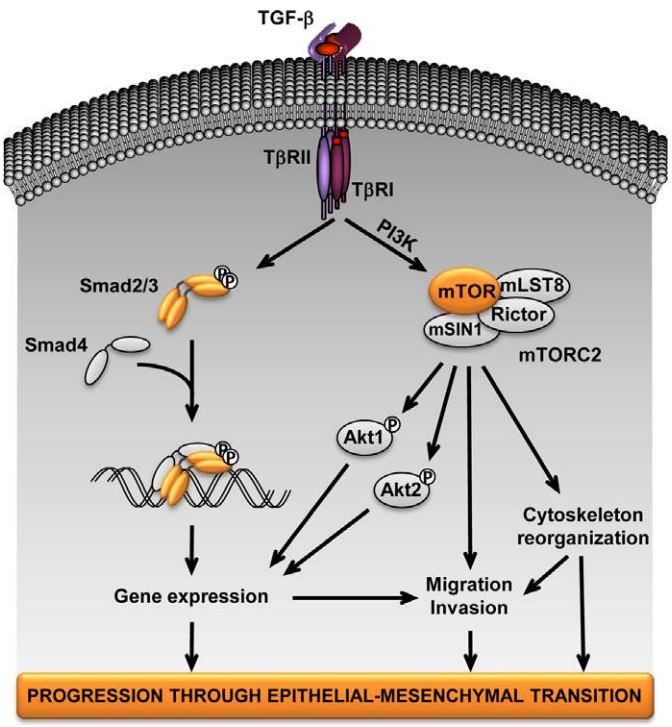

Fig. 8. Schematic diagram of the contribution of mTORC2 to TGF-β-induced EMT.

and decreased expression of α-smooth muscle actin (Gulhati et al., 2011). However, that study did not examine its role in EMT.

Role of mTORC2 in TGF-β signaling

In addition to Smad signaling, which directly impacts transcription, TGF-β induces ERK, p38 and JNK MAPK signaling (Derynck and Zhang, 2003; Moustakas and Heldin, 2005). It also induces mTORC1 signaling through PI3K and Akt, in cells undergoing EMT (Lamouille and Derynck, 2007). We now show that TGF-β additionally induces mTORC2 kinase activity to mediate phosphorylation of Akt(S473) in cells undergoing EMT. Blocking PI3K prevented TGF-β-induced mTORC2 activation and Akt(S473) phosphorylation, suggesting that mTORC2 activation in response to TGF-β occurs through PI3K. The mechanisms that lead to mTORC2 activation remain largely unknown.

Our findings place mTORC2 as a functional complex in TGF-β signaling and a central regulator of EMT responses. Early in TGF-β-induced EMT, mTORC2 induces the expression of Snail, which represses E-cadherin transcription. Moreover, mTORC2 is required for TGF-β-induced GSK-3β phosphorylation, an Akt target involved in the subcellular localization and function of Snail (Zhou et al., 2004). Additionally, both Akt1 and Akt2 act as downstream targets of TGF-β-induced mTORC2 activation in the regulation of Snail and MMP9 expression. Previous reports identified distinct roles for Akt1 and Akt2 in the regulation of EMT, and/or invasion and metastatic potential (Irie et al., 2005; Iliopoulos et al., 2009). In another study, Akt1 is selectively activated by mTORC2, and decreased Akt1 expression correlates with decreased cancer cell migration, invasion and metastasis (Kim et al., 2011). These observations suggest that the contributions of Akt1 and Akt2 might vary, depending on the cell system and EMT inducer.

TGF-β is known to activate RhoA in a manner that is dependent upon the TβRI kinase (Fleming et al., 2009), and its downstream kinase $p160^{ROCK}$ in epithelial cells, and their activities are required for EMT (Bhowmick et al., 2001). How TβRI mechanistically links to RhoA was unclear. We now show that mTORC2 is required for TGF-β-induced RhoA activation. This result is consistent with previous findings that mTORC2 acts upstream of Rho-GTPases in the control of actin organization (Jacinto et al., 2004; Sarbassov et al., 2004). The molecular linkage of mTORC2 with RhoA activation remains to be defined.

Whereas mTORC2 contributes to Akt activation, and Akt acts upstream from mTORC1, inactivation of mTORC2 function does not necessarily linearly affect mTORC1 activity, as reported (Shiota et al., 2006; Jacinto et al., 2006; Yang et al., 2006) and confirmed by our data. This might reflect a lack of quantitative correlation between Akt phosphorylation and mTORC1 activity, and the role of other pathways, such as Ras–ERK–RSK signaling, in mTORC1 activation (Roux et al., 2004). We previously reported a role for mTORC1 in TGF-β-induced EMT, specifically in protein synthesis, cell size, migration and invasion. With our findings on the function of mTORC2 in TGF-β-induced EMT, we conclude that mTORC1 and mTORC2 complement each other during EMT with distinct roles, yet both contribute to increased cell migration and invasion.

mTORC2 is required for EMT-associated cell migration and invasion

Our results show that mTORC2 is required for cell migration and invasion, which normally accompany EMT. These results are consistent with the recent observation that repression of Rictor expression impairs the migration and invasion of two cancer cell lines (Gulhati et al., 2011). The decreased migration of Rictor-knockdown cells treated with TGF-β might relate to impaired actin reorganization because actin stress fibers function as engines in the back to front migration. The focal adhesion complexes associated with the actin cytoskeleton at the edges of migrating cells are essential for substrate attachment and detachment of the cell during migration. We found that mTORC2 regulates the dynamic localization of these focal adhesions during migration, as monitored by paxillin expression. Previous studies reported a role for mTORC2 regulation of paxillin activity (Jacinto et al., 2004).

We also provide evidence that mTORC2 activity has a key role in invasion. Increased cell invasion is controlled by the expression and activity of MMPs that degrade the extracellular matrix (Kessenbrock et al., 2010). Our findings suggest that mTORC2 exerts its role in invasion in part through upregulation of MMP9 expression. The induction of MMP9 expression was dependent on Snail, which is consistent with the activation of MMP9 expression by Snail (Jorda et al., 2005), and on Akt1 and Akt2. Because cells with silenced Rictor expression showed impaired upregulation of Snail expression, we propose that mTORC2 controls MMP9 expression through Snail, possibly with involvement of Akt1 and/or Akt2. How mTORC2 links to gene expression, and whether it crosstalks with TGF-β-activated Smads in regulating gene expression are questions for future studies.

Targeting mTORC2 in cancer dissemination

We also evaluated the role of mTORC2 in cancer cell dissemination. As model cell system we used E4 squamous

carcinoma cells, which undergo EMT in response to TGF-β, form TGF-β-dependent mesenchymal spindle tumors following subcutaneous injection in mice and disseminate to form lung metastatic nodules following tail vein injection. Our in vivo studies showed that inhibition of mTORC2 function caused the subcutaneous tumors to revert from an aggressive spindle cell to a squamous carcinoma phenotype, as apparent by E-cadherin staining, and dramatically prevented cancer dissemination and metastatic growth in the lung. Our results complement recent observations that inactivation of mTORC2, by attenuation of Rictor expression, interferes with prostate tumor growth through inhibition of cell proliferation and survival (Guertin et al., 2009) and with dissemination of KM20 colon cancer cells in nude mice (Gulhati et al., 2011).

Loss of epithelial characteristics and acquisition of mesenchymal properties, are thought to be at the basis of carcinoma cell invasion and progression, leading to metastasis (Thiery and Sleeman, 2006). Upregulation of autocrine TGF-β signaling, resulting from increased production of active TGF-β and increased cell surface TGF-β levels on tumor cells, has an important role in this epithelial plasticity response (Bierie and Moses, 2006b). Our findings suggest that inhibition of mTORC2 activity might prevent cancer progression by interfering with EMT, which serves as a basis of cancer invasion, metastasis and cancer stem cell generation. Importantly, inhibition of mTORC2 function might not affect the integrity of epithelial cells.

Materials and Methods

Cell culture, reagents and antibodies

NMuMG, D3 and E4 cells were cultured in DMEM with 10% FBS. NMuMG culture medium was supplemented with 10 μg/ml insulin (Sigma) for maintenance only. Cells were treated with 2 ng/ml TGF-β1 (Peprotech or HumanZyme) or 5 μg/ml of insulin (Sigma). The TβRI kinase inhibitor SB431542 (Sigma) was used at 5 μM without TGF-β treatment to inhibit secreted autocrine TGF-β, or 1 hour before cell treatment. LY294002 (Sigma-Aldrich), GDC-0941 (Selleck Chemicals) and rapamycin (Calbiochem) were used at 10 μM, 1 μM, and 100 nM respectively, 1 hour before cell treatment.

Antibodies used were specific for phosphorylated Akt(Ser473) and Akt(Thr308), total Akt, Akt1, Akt2, phosphorylated Smad3, Smad3, phosphorylated GSK-3β(Ser9), phosphorylated S6(Ser235/236), phosphorylated S6(Ser240/244), S6, mTOR, Snail (Cell Signaling Technology), Rictor, mSIN1, mLST8, Raptor (Bethyl Laboratories), Rictor (Abcam), E-cadherin, GSK-3β (BD Transduction Laboratories), N-cadherin, fibronectin, α-tubulin (Sigma), RhoA (Cytoskeleton) and GAPDH (Santa Cruz Biotechnology).

Expression plasmids and transfection

Cells were transfected using LipofectAMINE PLUS (Invitrogen) with pEGFP–actin (Clontech, gift from Torsten Wittmann, University of California at San Francisco, San Francisco, CA) or pEGFP–paxillin (gift from Christopher Turner, State University of New York Upstate Medical University, Syracuse, NY) (West et al., 2001), following the manufacturer's instructions. For stable expression of luciferase and GFP, E4 cells were infected with pLV430G-oFL-T2A-eGFP, a lentivirus expressing the luciferase gene cloned in a EGFP expressing vector (gift from Brian Rabinovich, The University of Texas M. D. Anderson Cancer Center, Houston, TX), and GFP-positive cells were sorted by flow cytometry 1 week after infection.

RNA interference

To stably downregulate the expression of Rictor, mSIN1 or Snail, cells were infected with lentivirus expressing shRNAs to Rictor, mSIN1 or Snail (TRC shRNA library, Sigma), and the lentiviral empty vector pLKO.1 or TurboGFP shRNA control vector were used to derive the control cells. The cells were then selected with puromycin (InvivoGen) for 1 week before experimentation. To transiently downregulate the expression of ILK, Akt1, Akt2 or MMP9, cells were transfected for 72 hours with validated siRNA (Qiagen), and siRNA Control was used to derive the control cells. siRNA transfection was performed using Lipofectamine RNAiMAX (Invitrogen), following the manufacturer's instructions.

shRNA sequences used were: shRictor#1, 5′-CCGGCGAGACTTTGTCTGTCTAATTCTCGAGAATTAGACAGACAAAGTCTCGTTTTTG-3′; shRictor#2, 5′-CCGGGCCATCTGAATAACTTCACTACTCGAGTAGTGAAGTTATTCAGATGGCTTTTTG-3′; shmSIN1#1, 5′-CCGGGCCCATTCATAAGTTTGGCTTCTCGAGAAGCCAAACTTATGAATGGCTTTTTG-3′; shmSIN1#2, 5′-CCGGCCCAGTCTGTTGATATTACATCTCGAGATGTAATATCAACAGACTGGGTTTTTG-3′; shSnail, 5′-CCGGCCAAACCCACTCGGATGTGAACTCGAGTTCACATCCGAGTGGGTTTGGTTTTTG-3′; shAkt1, 5′-CCGGTCTGAGACTGACACCAGGTATCTCGAGATACCTGGTGTCAGTCTCAGATTTTTG-3′; shAkt2, 5′-CCGGCGACCCAACACCTTTGTCATACTCGAGTATGACAAAGGTGTTGGGTCGTTTTTG-3′. siRNA sequences used are: siILK, 5′-CCGCAGTGTAATGATCGATGA-3′; siAkt1, 5′-AACGGACTTCGGGCTGTGCAA-3′; siAkt2, 5′-CTGGCAGGACGTGGTACAGAA-3′; siMMP9, 5′-CAACCGCTGCATAAATATTAA-3′.

Immunoblotting

Cells were lysed in RIPA buffer with protease and phosphatase inhibitors. Protein concentration was determined using a modified Bradford protein assay (Bio-Rad). 20 μg of protein was separated by SDS-PAGE and transferred to nitrocellulose membranes which were blocked with 5% dry milk TBST for 1 h before overnight incubation with primary antibody diluted in 3% BSA in TBST. HRP-conjugated secondary antibody (Jackson ImmunoResearch Laboratories) was applied and detected by ECL (GE Healthcare) and BioMax film (Kodak).

RNA extraction and quantitative RT-PCR

After 1 hour, 24 hours or 48 hours in the presence or absence of TGF-β, RNA was extracted using the RNeasy mini kit (Qiagen). cDNA was generated using the iScript cDNA synthesis kit (Bio-Rad) and real-time PCR analysis performed for E-cadherin, Snail, MMP9 with iQ SYBR Green supermix (Bio-Rad) using RPL19 for normalization. The DNA Engine Opticon 2 cycler or a CFX96 Real-Time PCR detection system (Bio-Rad) with MJ Opticon Monitor analysis software and CFX Manager software (Bio-Rad) were used.

Primer sequences used were: E-cadherin, 5′-CAGGTCTCCTCATGGCTTTGC-3′ and 5′-CTTCCGAAAAGAAGGCTGTCC-3′; Snail, 5′-AAGATGCACATCCGAAGC-3′ and 5′-ATCTCTTCACATCCGAGTGG-3′; MMP9, 5′-GGACCCGAAGCGGACATTG-3′ and 5′-CGTCGTCGAAATGGGCATCT-3′; RPL19, 5′-ATGAGTATGCTCAGGCTACAGA-3′ and 5′-GCATTGGCGATTTCATTGGTC-3′.

Migration assay

Cells were treated without or with TGF-β to induce EMT for 48 hours and confluent monolayers wounded with a plastic tip in DMEM with 0.2% FBS. Cells were either observed by phase contrast or immunofluorescence microscopy after 3 hours or 6 hours.

Invasion assay

After adding TGF-β or not for 48 hours, cells were trypsinized and 50,000 cells added to Matrigel-coated inserts (BioCoat Matrigel Invasion Chamber; Becton Dickinson) in DMEM with 0.2% FBS. These were then placed in companion plates with DMEM 10% FBS for 24 hours. Cells in upper chambers were removed, filters were fixed in methanol 5 minutes at −20℃, and mounted using ProLong Gold antifade reagent with DAPI (Invitrogen).

RhoA-GTP pulldown assay

Cells were cultured for 12 hours in DMEM with 1% FBS, starved for 4 hours in serum-free medium, and TGF-β was added or not for 5 or 10 minutes before using a RhoA activation assay kit (Cytoskeleton). Briefly, cells were lysed, protein concentration determined, and 600 μg of protein was incubated for 1 hour with 50 μg of Rhotekin-RBD–Sepharose beads at 4℃. Beads were washed and GTP-bound RhoA was detected by SDS-PAGE and western blotting.

Zymography

Cells were cultured in serum-free medium for 12 hours and TGF-β and/or SB431542 were added or not for 24 hours. Cells were lysed in RIPA buffer and medium was clarified by centrifugation and concentrated using Microcon Ultracel YM-10 (Millipore). Protein concentrations were determined and normalized, and 5 μg of protein was resolved by SDS-PAGE containing 0.1% gelatin. Gels were washed and incubated overnight at 37℃ in gelatinase buffer (50 mM Tris-HCl, pH 7.4, 5 mM $CaCl_2$, 1 μM $ZnCl_2$) before staining with Coomassie Brilliant Blue.

Immunoprecipitation, co-immunoprecipitation and kinase assay

Cells were lysed in ice-cold lysis buffer (20 mM Tris-HCl, 150 mM NaCl, 0.5% Triton X-100 or 0.3% CHAPS for co-immunoprecipitation and kinase assay) with protease and phosphatase inhibitors. 500 μg to 1 mg of protein was precleared with 10 μl of Protein-G–Sepharose (GE Healthcare) for 1 hour, and then immunoprecipitated for 2 hours. Protein-G–Sepharose (20 μl) was added to each reaction, tubes were rotated for 1 hour at 4℃, and beads washed in 1 ml lysis buffer four times for 10 minutes. For the mTORC2 kinase assay, an additional rictor-mTOR kinase buffer [25 mM HEPES (pH 7.5), 100 mM potassium acetate,

and 2 mM $MgCl_2$] wash was performed. Immunoprecipitates were then incubated with 500 ng full-length inactive Akt1–GST (SignalChem) and 500 μM ATP at 37℃ for 40 minutes. Bound proteins were eluted from beads and analyzed by SDS-PAGE and western blotting.

Immunofluorescence

Cells were fixed with 4% paraformaldehyde (PFA) for 30 minutes, permeabilized in 2% PFA and 0.2% Triton X-100 for 10 minutes, and blocked with 3% BSA for 1 hour. E-cadherin, paxillin (BD Transduction Laboratories) or α-tubulin (Sigma) in 3% BSA were added for 2 hours, and detected using secondary antibodies conjugated to Alexa Fluor 488 or Alexa Fluor 647, with Alexa-Fluor-555–phalloidin (Invitrogen) to visualize actin filaments. Slides were mounted using ProLong Gold anti-fade reagent with DAPI (Invitrogen).

Cell imaging

To view the cell morphology or monitor TGF-β-induced EMT, cells were observed using a phase-contrast microscope (Diaphot; Nikon) and pictures were acquired using a Nikon D2x camera with a 20× NA 0.4 air objective, and analyzed using Photoshop software (Adobe). To monitor cell migration, cells were observed using a Leica DMI 4000B microscope, and bright-field pictures were taken at 24 hours and 48 hours using a Leica DFC 350FX camera. Images were analyzed using the Leica Application Suite software. After cell fixation and immunofluorescence staining, images were acquired using a Nikon T*i* inverted microscope with 100×/1.49 or 60×/1.49 Apo TIRF objectives and Coolsnap HQ^2 camera (Photometrics) controlled by NIS Elements software (Nikon).

For live-cell imaging, cells were maintained in Hank's balanced salts solution (HBSS; Invitrogen) with 10% FBS at 37℃. For wide-field epifluorescence microscopy, images were acquired using a Nikon T*i* inverted microscope with a 100×/1.49 or 60×/1.49 Apo TIRF objective and Coolsnap HQ^2 camera controlled by NIS Elements software. For GFP-tagged actin dynamics, images were acquired every 5 minutes (200 msecond exposure) for 60 minutes. In addition, single time point *Z*-stacks of GFP-tagged actin were acquired and deconvolution was performed using Autoquant software (Media Cybernetics). Stress fiber density was quantified from linear fluorescence intensity profiles generated by drawing lines through cell bodies using ImageJ software (NIH) and expressed as number of peaks (stress fibers) per 10 μm. Data from three such profiles were generated per cell and averaged. ImageJ was also used to determine stress fiber angles (five per cell) and circular statistical analysis performed using Oriana 3 software (Kovach) to quantify stress fiber alignment within individual cells (Kaunas et al., 2005).

For TIRFm of GFP-tagged paxillin, through-the-objective TIRF illumination was achieved using a 486 nm DPSS laser source (Spectral Applied Research), and a Cascade II 512 camera (Photometrics). For GFP-tagged paxillin dynamics, images were acquired every 60 seconds (200 msecond exposure) for 30 minutes. Additional image processing was performed using ImageJ software (NIH).

In vivo tumorigenesis assays

6- to 8-week-old female *nu/nu* mice were used in accordance with a protocol approved by the UCSF IACUC. Animals were sacrificed by cervical dislocation. For xenografts, 5×10^6 E4 cells were injected subcutaneously at two sites into anaesthetized mice. At 3 weeks, mice were injected intraperitoneally with BrdU 5 mg/ml (5-bromo-2-deoxyuridine; Sigma) 2 hours before tumor collection. Two independent xenograft experiments were performed with $n=7$ mice each for control and Rictor-knockdown cells in the first experiment, and $n=4$ mice for the second. For lateral tail vein injections, 1×10^6 E4 cells were administered and injections confirmed by immediate bioluminescence imaging following the Xenogen protocol. Bioluminescence was monitored weekly (see tumor imaging section). For BLI plots, photon flux was calculated for each mouse using a rectangular region of interest encompassing the thorax of the mouse in a prone position. At 29 days, mice were injected intraperitoneally with BrdU 5 mg/ml for 2 hours, sacrificed, and whole lungs viewed by stereo dissection microscopy. Two independent tail vein injection experiments were performed with $n=7$ mice each for control and Rictor-knockdown conditions in the first experiment, and $n=5$ mice for the second.

Tumor imaging

In the xenograft experiment, quantification of E-cadherin was performed by capturing ten fields of view per mouse tumor at 20× magnification using an Olympus BX60 microscope with an Olympus DP71 camera and the software DP Controller. The total area of the field and the E-cadherin-positive region were determined using ImageJ (NIH). For BrdU and TUNEL staining, the number of positive cells per field of view was calculated using ImageJ. Quantification was performed by capturing ten fields of view per sample at 20× magnification using an Olympus BX60 microscope with Olympus DP71 camera and DP Controller software.

In the tail vein injection experiment, whole lungs were viewed under a fluorescence dissection microscope Leica MZH-III, with a camera QImage Micropublisher 5.0, and the number of GFP-positive foci was analyzed using the software QImage. For bioluminescence imaging, mice were anesthetized by inhalation of 3% isoflurane/oxygen mixture delivered by the Xenogen XGI-85-port gas anesthesia system, and injected with 3 mg of d-luciferin (Gold Bio Technology). Imaging and image analysis were performed following the Xenogen protocol using a cooled CCD camera system (IVIS-100; Xenogen) and LivingImage software (Xenogen).

Tumor analysis

For analysis of proteins from tumor tissue, frozen tumors were ground to a fine powder using a mortar and pestle over liquid nitrogen. Proteins were solubilized in RIPA buffer containing phosphatase and protease inhibitors, and insoluble material removed by centrifugation. Protein levels were normalized using a modified Bradford protein assay (Bio-Rad) and the lysate was analyzed by SDS-PAGE and immunoblotting.

Immunohistochemistry was performed on tissues fixed in 4% PFA. Tissues were embedded in paraffin and 5 μm sections were deparaffinized, rehydrated through graded alcohols, and subjected to antigen retrieval for immunohistochemistry. Sections were incubated with an antibody against E-cadherin (BD Transduction Laboratories). Immune complexes were visualized by the ABC peroxidase method (Vector Laboratories), and sections were counterstained with hematoxylin. For immunofluorescence of tumor sections, tissue was embedded in OCT compound (Tissue-Tek) and snap frozen. Sections were fixed in methanol and acetone (1:1), incubated with antibodies against E-cadherin (BD Transduction Laboratories), Rictor (Bethyl Laboratories) or GFP (Rockland), stained with Alexa-Fluor-488-conjugated secondary antibody (Invitrogen), and counterstained with DAPI. For proliferation analysis, tissues from BrdU-treated animals were deparaffinized, rehydrated through graded alcohols, subjected to antigen retrieval, and treated with HCl for immunohistochemistry. Sections were incubated anti-BrdU Alexa Fluor 594 (Invitrogen) and counterstained with DAPI. For tail vein studies, lung tissue was embedded in OCT compound (Tissue-Tek), snap-frozen, and sections fixed using 1:1 methanol and acetone, followed by antigen retrieval/HCl treatment. Sections were incubated with anti-BrdU Alexa Fluor 594 (Invitrogen) and anti-GFP (Rockland). GFP was visualized using secondary antibodies conjugated to Alexa Fluor 488 (Invitrogen). Apoptosis was determined using the In Situ Cell Death Detection Kit (Roche). Briefly, frozen tissue sections were fixed in 1:1 methanol and acetone, permeabilized, and incubated with TUNEL fluorescent labeling reagent.

Statistics

All quantitative data were analyzed using Prism 5 software (GraphPad) and expressed as mean ± s.e.m. A two-tailed unpaired Student's *t*-test was used to analyze data containing two groups; $P<0.05$ was deemed statistically significant.

Acknowledgements

We are grateful to Byron Hann, Paul Phojanakong and Donghui Wang of the HDFCCC Preclinical Therapeutics Core for assistance, and Angela DeSapio and Honrado Lopez for help with the in vivo studies, Tara Rambaldo from the UCSF Cell Analysis Core for assistance, Robin Shaw for access to fluorescence microscopy, Brian Rabinovich, Torsten Wittmann, Christopher Turner for gifts of reporter plasmids and Lutz Kockel for critical review of the manuscript.

Funding

This research was supported by the National Institutes of Health [grant numbers RO1-CA136690 and PO1-HL60231 (project III) to R.D.; RO1-CA116019, RO1-HL078564 and RO1-GM60514 to R.J.A.]; a Leukemia and Lymphoma Society postdoctoral fellowship [grant number 5566-07] and an American Heart Association scientist development award [grant number SDG2280008] to S.L.; a postdoctoral support from the National Cancer Institute [grant number T32 CA108462] to E.C.; a postdoctoral fellowship from the American Federation for Aging Research [grant number A112457] and an American Heart Association scientist development award [grant number SDG3420042] to J.W.S. Deposited in PMC for release after 12 months.

Supplementary material available online at
http://jcs.biologists.org/lookup/suppl/doi:10.1242/jcs.095299/-/DC1

References

Bhowmick, N. A., Ghiassi, M., Bakin, A., Aakre, M., Lundquist, C. A., Engel, M. E., Arteaga, C. L. and Moses, H. L. (2001). Transforming growth factor-β1 mediates epithelial to mesenchymal transdifferentiation through a RhoA-dependent mechanism. *Mol. Biol. Cell* **12**, 27-36.

Bierie, B. and Moses, H. L. (2006a). TGF-β and cancer. *Cytokine Growth Factor. Rev.* **17**, 29-40.

Bierie, B. and Moses, H. L. (2006b). Tumour microenvironment: TGFβ: the molecular Jekyll and Hyde of cancer. *Nat. Rev. Cancer* **6**, 506-520.

Burns, P. A., Kemp, C. J., Gannon, J. V., Lane, D. P., Bremner, R. and Balmain, A. (1991). Loss of heterozygosity and mutational alterations of the p53 gene in skin tumours of interspecific hybrid mice. *Oncogene* **6**, 2363-2369.

Deakin, N. O. and Turner, C. E. (2008). Paxillin comes of age. *J. Cell Sci*. **121**, 2435-2444.

Derynck, R. and Zhang, Y. E. (2003). Smad-dependent and Smad-independent pathways in TGF-β family signalling. *Nature* **425**, 577-584.

Feng, X. H. and Derynck, R. (2005). Specificity and versatility in TGF-β signaling through Smads. *Annu. Rev. Cell Dev. Biol.* **21**, 659-693.

Fleming, Y. M., Ferguson, G. J., Spender, L. C., Larsson, J., Karlsson, S., Ozanne, B. W., Grosse, R. and Inman, G. J. (2009). TGF-β-mediated activation of RhoA signalling is required for efficient ^{V12}HaRas and ^{V600E}BRAF transformation. *Oncogene* **28**, 983-993.

Frias, M. A., Thoreen, C. C., Jaffe, J. D., Schroder, W., Sculley, T., Carr, S. A. and Sabatini, D. M. (2006). mSin1 is necessary for Akt/PKB phosphorylation, and its isoforms define three distinct mTORC2s. *Curr. Biol*. **16**, 1865-1870.

Guertin, D. A., Stevens, D. M., Thoreen, C. C., Burds, A. A., Kalaany, N. Y., Moffat, J., Brown, M., Fitzgerald, K. J. and Sabatini, D. M. (2006). Ablation in mice of the mTORC components raptor, rictor, or mLST8 reveals that mTORC2 is required for signaling to Akt-FOXO and PKCα, but not S6K1. *Dev. Cell* **11**, 859-871.

Guertin, D. A., Stevens, D. M., Saitoh, M., Kinkel, S., Crosby, K., Sheen, J. H., Mullholland, D. J., Magnuson, M. A., Wu, H. and Sabatini, D. M. (2009). mTOR complex 2 is required for the development of prostate cancer induced by Pten loss in mice. *Cancer Cell*. **15**, 148-159.

Gulhati, P., Bowen, K. A., Liu, J., Stevens, P. D., Rychahou, P. G., Chen, M., Lee, E. Y., Weiss, H. L., O'Connor, K. L., Gao, T. and Evers, B. M. (2011). mTORC1 and mTORC2 regulate EMT, motility, and metastasis of colorectal cancer via RhoA and Rac1 signaling pathways. *Cancer Res*. **71**, 3246-3256.

Iliopoulos, D., Polytarchou, C., Hatziapostolou, M., Kottakis, F., Maroulakou, I. G., Struhl, K. and Tsichlis, P. N. (2009). MicroRNAs differentially regulated by Akt isoforms control EMT and stem cell renewal in cancer cells. *Sci. Signal*. **2**, ra62.

Irie, H. Y., Pearline, R. V., Grueneberg, D., Hsia, M., Ravichandran, P., Kothari, N., Natesan, S. and Brugge, J. S. (2005). Distinct roles of Akt1 and Akt2 in regulating cell migration and epithelial-mesenchymal transition. *J. Cell Biol*. **171**, 1023-1034.

Jacinto, E., Loewith, R., Schmidt, A., Lin, S., Ruegg, M. A., Hall, A. and Hall, M. N. (2004). Mammalian TOR complex 2 controls the actin cytoskeleton and is rapamycin insensitive. *Nat. Cell Biol*. **6**, 1122-1128.

Jacinto, E., Facchinetti, V., Liu, D., Soto, N., Wei, S., Jung, S. Y., Huang, Q., Qin, J. and Su, B. (2006). SIN1/MIP1 maintains rictor-mTOR complex integrity and regulates Akt phosphorylation and substrate specificity. *Cell* **127**, 125-137.

Jorda, M., Olmeda, D., Vinyals, A., Valero, E., Cubillo, E., Llorens, A., Cano, A. and Fabra, A. (2005). Upregulation of MMP-9 in MDCK epithelial cell line in response to expression of the Snail transcription factor. *J. Cell Sci*. **118**, 3371-3385.

Kaunas, R., Nguyen, P., Usami, S. and Chien, S. (2005). Cooperative effects of Rho and mechanical stretch on stress fiber organization. *Proc. Natl. Acad. Sci. USA* **102**, 15895-15900.

Kessenbrock, K., Plaks, V. and Werb, Z. (2010). Matrix metalloproteinases: regulators of the tumor microenvironment. *Cell* **141**, 52-67.

Kim, E. K., Yun, S. J., Ha, J. M., Kim, Y. W., Jin, I. H., Yun, J., Shin, H. K., Song, S. H., Kim, J. H., Lee, J. S., Kim, C. D. and Bae, S. S. (2011). Selective activation of Akt1 by mammalian target of rapamycin complex 2 regulates cancer cell migration, invasion, and metastasis. *Oncogene* **30**, 2954-2963

Klymkowsky, M. W. and Savagner, P. (2009). Epithelial-mesenchymal transition: a cancer researcher's conceptual friend and foe. *Am. J. Pathol*. **174**, 1588-1593.

Lamouille, S. and Derynck, R. (2007). Cell size and invasion in TGF-β-induced epithelial to mesenchymal transition is regulated by activation of the mTOR pathway. *J. Cell Biol*. **178**, 437-451.

Laplante, M. and Sabatini, D. M. (2009). mTOR signaling at a glance. *J. Cell Sci*. **122**, 3589-3594.

McDonald, P. C., Oloumi, A., Mills, J., Dobreva, I., Maidan, M., Gray, V., Wederell, E. D., Bally, M. B., Foster, L. J. and Dedhar, S. (2008). Rictor and integrin-linked kinase interact and regulate Akt phosphorylation and cancer cell survival. *Cancer Res*. **68**, 1618-1624.

Miettinen, P. J., Ebner, R., Lopez, A. R. and Derynck, R. (1994). TGF-β induced transdifferentiation of mammary epithelial cells to mesenchymal cells: involvement of type I receptors. *J. Cell Biol*. **127**, 2021-2036.

Miyazono, K. (2009). Transforming growth factor-β signaling in epithelial-mesenchymal transition and progression of cancer. *Proc. Jpn. Acad. Ser. B. Phys. Biol. Sci*. **85**, 314-323.

Moustakas, A. and Heldin, C. H. (2005). Non-Smad TGF-β signals. *J. Cell Sci*. **118**, 3573-3584.

Moustakas, A. and Heldin, C. H. (2007). Signaling networks guiding epithelial-mesenchymal transitions during embryogenesis and cancer progression. *Cancer Sci*. **98**, 1512-1520.

Nguyen, D. X. and Massagué, J. (2007). Genetic determinants of cancer metastasis. *Nat. Rev. Genet*. **8**, 341-352.

Ozdamar, B., Bose, R., Barrios-Rodiles, M., Wang, H. R., Zhang, Y. and Wrana, J. L. (2005). Regulation of the polarity protein Par6 by TGFβ receptors controls epithelial cell plasticity. *Science*. **307**, 1603-1609.

Padua, D. and Massagué, J. (2009). Roles of TGFβ in metastasis. *Cell Res*. **19**, 89-102.

Portella, G., Cumming, S. A., Liddell, J., Cui, W., Ireland, H., Akhurst, R. J. and Balmain, A. (1998). Transforming growth factor β is essential for spindle cell conversion of mouse skin carcinoma in vivo: implications for tumor invasion. *Cell Growth Differ*. **9**, 393-404.

Roux, P. P., Ballif, B. A., Anjum, R., Gygi, S. P. and Blenis, J. (2004). Tumor-promoting phorbol esters and activated Ras inactivate the tuberous sclerosis tumor suppressor complex via p90 ribosomal S6 kinase. *Proc. Natl. Acad. Sci. USA* **101**, 13489-13494.

Sarbassov, D. D., Ali, S. M., Kim, D. H., Guertin, D. A., Latek, R. R., Erdjument-Bromage, H., Tempst, P. and Sabatini, D. M. (2004). Rictor, a novel binding partner of mTOR, defines a rapamycin-insensitive and raptor-independent pathway that regulates the cytoskeleton. *Curr. Biol*. **14**, 1296-1302.

Sarbassov, D. D., Guertin, D. A., Ali, S. M. and Sabatini, D. M. (2005). Phosphorylation and regulation of Akt/PKB by the rictor-mTOR complex. *Science* **307**, 1098-1101.

Shi, Y. and Massagué, J. (2003). Mechanisms of TGF-β signaling from cell membrane to the nucleus. *Cell* **113**, 685-700.

Shiota, C., Woo, J. T., Lindner, J., Shelton, K. D. and Magnuson, M. A. (2006). Multiallelic disruption of the rictor gene in mice reveals that mTOR complex 2 is essential for fetal growth and viability. *Dev. Cell* **11**, 583-589.

Thiery, J. P. and Sleeman, J. P. (2006). Complex networks orchestrate epithelial-mesenchymal transitions. *Nat. Rev. Mol. Cell Biol*. **7**, 131-142.

Thiery, J. P., Acloque, H., Huang, R. Y. and Nieto, M. A. (2009). Epithelial-mesenchymal transitions in development and disease. *Cell* **139**, 871-890.

West, K. A., Zhang, H., Brown, M. C., Nikolopoulos, S. N., Riedy, M. C., Horwitz, A. F. and Turner, C. E. (2001). The LD4 motif of paxillin regulates cell spreading and motility through an interaction with paxillin kinase linker (PKL). *J. Cell Biol*. **154**, 161-176.

Xu, J., Lamouille, S. and Derynck, R. (2009). TGF-β-induced epithelial to mesenchymal transition. *Cell Res*. **19**, 156-172.

Yang, Q., Inoki, K., Ikenoue, T. and Guan, K. L. (2006). Identification of Sin1 as an essential TORC2 component required for complex formation and kinase activity. *Genes Dev*. **20**, 2820-2832.

Yilmaz, M. and Christofori, G. (2009). EMT, the cytoskeleton, and cancer cell invasion. *Cancer Metastasis Rev*. **28**, 15-33.

Zavadil, J. and Böttinger, E. P. (2005). TGF-β and epithelial-to-mesenchymal transitions. *Oncogene* **24**, 5764-5774.

Zeisberg, M. and Neilson, E. G. (2009). Biomarkers for epithelial-mesenchymal transitions. *J. Clin. Invest*. **119**, 1429-1437.

Zhou, B. P., Deng, J., Xia, W., Xu, J., Li, Y. M., Gunduz, M. and Hung, M. C. (2004). Dual regulation of Snail by GSK-3beta-mediated phosphorylation in control of epithelial-mesenchymal transition. *Nat. Cell Biol*. **6**, 931-940.